Prediction of Helicopter Maneuver Loads Using BDF/Time Spectral Method on Unstructured Meshes

Zhi Yang * Dimitri J. Mavriplis †
Jayanarayanan Sitaraman ‡
Department of Mechanical Engineering, University of Wyoming, Laramie, WY 82071

For flows with strong periodic content, time-spectral methods can be used to obtain time-accurate solutions at substantially reduced cost compared to traditional time-implicit methods which operate directly in the time domain. The time-spectral approach requires the simultaneous coupled solution of multiple time instances, which can be performed effectively in parallel on modern multicore parallel computer architectures. Although time-spectral methods are only applicable to purely periodic flows, in previous work we have demonstrated the ability of a hybrid BDF/time-spectral approach for simulating quasi-periodic flows with good overall efficiency. A quasi periodic flow is defined as one which involves a slow transient in addition to a higher frequency periodic component. In this paper, we apply the BDF/time-spectral approach to compute the important practical problem of time dependent helicopter maneuver loads, which combine the periodic rotor motion with a slower vehicle maneuvering transient. The simulation includes a rotating and deforming mesh with prescribed aeroelastic blade deflections. The formulated BDF/time-spectral approach is compliant with the geometric conservation law, and produces equivalent temporal accuracy using less computation effort compared to a traditional BDF time-implicit approach.

I. Introduction

Unstructured mesh approaches have become well established for steady-state flow simulations due to the flexibility they afford for dealing with complex geometries. For unsteady flows with moving boundaries, such as aeroelastic problems, implicit time-integration strategies are required for the efficient solution of the flow equations. However, for problems with strong periodic content, such as turbomachinery flows or rotorcraft aerodynamics, time-spectral methods can be used to substantially reduce the cost of computing the full time-dependent solution for a given level of accuracy.

The time spectral method is based on the use of discrete Fourier analysis. McMullen[22,23] used the harmonic balance technique to transform the unsteady equations in the physical domain to a set of steady equations in the frequency domain. Subsequently, Gopinath[10,30] proposed to solve the unsteady equations in the time domain by applying the time discretization operator. The time spectral method was shown to be faster than the dual-time stepping implicit methods using backwards difference time formulae for time periodic computations, such as turbomachinery flows,[22,30] oscillatory pitching airfoil/wing cases,[10,16] flapping wing,[24] helicopter rotor[7,8] and vortex shedding problems.[23]

In practice, the time spectral method can only be applied to periodic flows. However, there are many quasi-periodic flows which combine strong periodic content with a slow mean flow transient, such as an oscillating pitching and climbing airfoil or wing, and a maneuvering helicopter rotor. In such cases, practical time-stepping simulations can become very costly since the time step is limited by the accuracy considerations imposed by the fast periodic flow features (i.e. time steps typically smaller than 1 degree of rotation for rotorcraft configurations) while long time histories must be simulated to capture the slower transient effects.

*Research Scientist, AIAA member; email: zyang@uwyo.edu
†Professor, AIAA Associate Fellow; email: mavriplis@uwyo.edu
‡Assistant Professor, AIAA member; email: jsitaram@uwyo.edu

In previous work, we have introduced a hybrid BDF/time-spectral approach which aims to simulate quasi-periodic flows with slow transients combined with relatively fast periodic content using global BDF time step sizes of the order of the period length, while making use of the properties of the time-spectral approach to capture accurate details of the periodic flow components.[20] The idea is rooted in the concept of polynomial subtraction for spectral methods, discussed by Gottlieb and Orzag[11] and originally credited to Lanczos.[15] In this approach, the non-periodic (transient) portion of a quasi-periodic function is subtracted from the function and represented with a polynomial basis set. The remaining function is periodic and thus can be approximated efficiently with spectral basis functions. In order to be practical, the BDF/time-spectral approach must be applicable to problems with moving and deforming meshes. These methods must also preserve important properties such as discrete conservation in the presence of dynamically deforming meshes, and techniques for efficiently solving the large implicit systems arising at each time step must be employed.

When explicit algorithms are used to integrate the time-spectral or BDF/time-spectral approaches in pseudo time, small (pseudo) time steps must be used due to stability considerations. Furthermore, as the number of time instances or harmonics increases, the time-step restriction becomes more severe and the convergence rate decreases as well.[12] In this work, we make use of an efficient block-Jacobi implicit method originally presented by Sicot[25] to alleviate this dependence of the convergence rate on the number of harmonics.

The various time instances or harmonic solutions in the time spectral approach are coupled and must be solved simultaneously. However, the coupling only comes in through a source term and each individual time instance may be solved in parallel with the other time instances. This introduces an additional dimension for achieving parallelism compared to time-domain computations, where progress in the time dimension is necessarily sequential. In our implementation, two levels of parallelism are introduced, the first in the spatial dimension, and the second in the time dimension where the various time instances are solved by spawning multiple instances of the spatial solver on a parallel computer. The implementation is performed with minimal modifications to an existing steady-state unstructured multigrid solver, and using multiple MPI communicators to manage communication for the coupling between the harmonic solution instances, and within each time instance solution in the spatial dimension.

In the following sections, we first outline the governing equations and the base flow solver. We then discuss the time spectral method and subsequently the hybrid BDF/time-spectral approach. This is followed by a formulation of the geometric conservation law (GCL), which must be verified in order to guarantee discrete conservation in the presence of dynamically deforming meshes. The BDF/time-spectral method is first demonstrated on a simple two-dimensional problem, and subsequently applied to the important practical problem of predicting helicopter maneuver loads by simulating a prescribed pull-up maneuver for the UH-60 flexible rotor, for which both previous BDF time-domain computational results[1–3,26,28] and flight-test data[4] are available for comparison.

II. Governing Equations

A. Base Solver

The Navier-Stokes equations in conservative form can be written as:

$$\frac{\partial \mathbf{U}}{\partial t} + \nabla \cdot (\mathbf{F}(\mathbf{U}) + \mathbf{G}(\mathbf{U})) = 0 \tag{1}$$

where $\mathbf{U}$ represents the vector of conserved quantities (mass, momentum, and energy), $\mathbf{F}(\mathbf{U})$ represents the convective fluxes and $\mathbf{G}(\mathbf{U})$ represents the viscous fluxes. Integrating over a (moving) control volume $\Omega(t)$, we obtain:

$$\int_{\Omega(t)} \frac{\partial \mathbf{U}}{\partial t} dV + \int_{\partial\Omega(t)} (\mathbf{F}(\mathbf{U}) \cdot \tilde{\mathbf{n}}) dS + \int_{\partial\Omega(t)} (\mathbf{G}(\mathbf{U}) \cdot \tilde{\mathbf{n}}) dS = 0 \tag{2}$$

Using the differential identity

$$\frac{\partial}{\partial t} \int_{\Omega(t)} \mathbf{U} dV = \int_{\Omega(t)} \frac{\partial \mathbf{U}}{\partial t} dV + \int_{\partial\Omega(t)} \mathbf{U}(\dot{\mathbf{x}} \cdot \tilde{\mathbf{n}}) dS \tag{3}$$

where $\dot{\mathbf{x}}$ and $\tilde{\mathbf{n}}$ are the velocity and normal of the interface $\partial\Omega(t)$, respectively, equation (2) becomes:

$$\frac{\partial}{\partial t}\int_{\Omega(t)} \mathbf{U}dV + \int_{\partial\Omega(t)} (\mathbf{F}(\mathbf{U}) - \mathbf{U}\dot{\mathbf{x}}) \cdot \tilde{\mathbf{n}}dS + \int_{\partial\Omega(t)} \mathbf{G}(\mathbf{U}) \cdot \tilde{\mathbf{n}}dS = 0 \tag{4}$$

Considering $\mathbf{U}$ as cell averaged quantities, these equations are discretized in space as:

$$\frac{\partial}{\partial t}(V\mathbf{U}) + \mathbf{R}(\mathbf{U}, \dot{\mathbf{x}}(\mathbf{t}), \tilde{\mathbf{n}}(\mathbf{t})) + \mathbf{S}(\mathbf{U}, \tilde{\mathbf{n}}(\mathbf{t})) = \mathbf{0} \tag{5}$$

where $\mathbf{R}(\mathbf{U}, \dot{\mathbf{x}}, \tilde{\mathbf{n}}) = \int_{\partial\Omega(t)} (\mathbf{F}(\mathbf{U}) - \dot{\mathbf{x}}\mathbf{U}) \cdot \tilde{\mathbf{n}}dS$ represents the discrete convective fluxes in ALE form, $S(\mathbf{U}, \tilde{\mathbf{n}})$ represents the discrete viscous fluxes, and V denotes the control volume. In the discrete form, $\dot{\mathbf{x}}(\mathbf{t})$ and $\tilde{\mathbf{n}}(\mathbf{t})$ now represent the time varying velocities and surface normals of the control-volume boundary faces.

The Navier-Stokes equations are discretized by a central difference finite-volume scheme with additional matrix-based artificial dissipation on hybrid meshes which may include tetrahedra, pyramids, prisms and hexahedra in three dimensions. Second-order accuracy is achieved using a two-pass construction of the artificial dissipation operator, which corresponds to an undivided biharmonic operator. A single unifying edge-based data-structure is used in the flow solver for all types of elements. For the base solver, the time derivative in equation (5) is discretized using a second order backwards difference (BDF2) scheme, resulting in a non-linear system to be solved at each time step. The implicit solution is achieved using a line-implicit agglomeration multigrid algorithm where a first-order accurate discretization is employed for the convective terms on coarse grid levels.[17,18]

B. Time Spectral Method

If the flow is periodic in time, the variables $\mathbf{U}$ can be represented by a discrete Fourier series. The discrete Fourier transform of $\mathbf{U}$ in a period of T is given by[10]

$$\widehat{\mathbf{U}}_k = \frac{1}{N}\sum_{n=0}^{N-1} \mathbf{U}^n e^{-ik\frac{2\pi}{T}n\Delta t} \tag{6}$$

where N is the number of time intervals and $\Delta t = T/N$. The Fourier inverse transform is then given as

$$\mathbf{U}^n = \sum_{k=-\frac{N}{2}}^{\frac{N}{2}-1} \widehat{\mathbf{U}}_k e^{ik\frac{2\pi}{T}n\Delta t} \tag{7}$$

Note that this corresponds to a collocation approximation, i.e. the function $\mathbf{U}(t)$ is projected into the space spanned by the truncated set of complex exponential (spectral) functions, and the expansion coefficients (in this case the $\widehat{\mathbf{U}}_k$) are determined by requiring $\mathbf{U}(t)$ to be equal to its projection at N discrete locations in time, as given by equations (6) and (7).
Differentiating equation (7) in time, we obtain:

$$\frac{\partial}{\partial t}(\mathbf{U}^n) = \frac{2\pi}{T}\sum_{k=-\frac{N}{2}}^{\frac{N}{2}-1} ik\widehat{\mathbf{U}}_k e^{ik\frac{2\pi}{T}n\Delta t} \tag{8}$$

Substituting equation (6) into equation (8), we get[6,13]

$$\frac{\partial}{\partial t}(\mathbf{U}^n) = \sum_{j=0}^{N-1} d_n^j \mathbf{U}^j \tag{9}$$

where

$$d_n^j = \begin{cases} \frac{2\pi}{T}\frac{1}{2}(-1)^{n-j}cot(\frac{\pi(n-j)}{N}) & n \neq j \\ 0 & n = j \end{cases}$$

for an even number of time instances and

$$d_n^j = \begin{cases} \frac{2\pi}{T}\frac{1}{2}(-1)^{n-j} cosec(\frac{\pi(n-j)}{N}) & n \neq j \\ 0 & n = j \end{cases}$$

for an odd number of time instances. The collocation approach for solving equation (5) consists of substituting the collocation approximation for the continuous function $\mathbf{U}(t)$ given by equation (7) into equation (5), and requiring equation (5) to hold exactly at the same N discrete locations in time (i.e. multiplying (5) by the dirac delta test function $\delta(t-t^n)$ and integrating over all time), yielding:

$$\sum_{j=0}^{N-1} d_n^j V^j \mathbf{U}^j + \mathbf{R}(\mathbf{U^n}, \dot{\mathbf{x}}^\mathbf{n}, \tilde{\mathbf{n}}^\mathbf{n}) + \mathbf{S}(\mathbf{U^n}, \tilde{\mathbf{n}}^\mathbf{n}) = 0 \qquad n = 0, 1, 2, ..., N-1 \tag{10}$$

This results in a system of N equations for the N time instances $\mathbf{U}^n$ which are all coupled through the summation over the time instances in the time derivative term. The spatial discretization operators remain unchanged in the time-spectral approach, with only the requirement that they be evaluated at the appropriate location in time. Thus, the time-spectral method may be implemented without any modifications to an existing spatial discretization, requiring only the addition of the temporal discretization coupling term, although the multiple time instances must be solved simultaneously due to this coupling.

C. Hybrid BDF/Time Spectral Method

The idea of polynomial subtraction for quasi-periodic functions is to subtract out the non-periodic transient, which can be modeled using a polynomial basis set, and to approximate the remaining purely periodic component with a spectral basis set.[11] From the point of view of a collocation method, this corresponds to using a mixed spectral/polynomial basis set for the projection of the continuous solution (in the time dimension).

We proceed by splitting the quasi-periodic temporal variation of the solution into a periodic and slowly varying mean flow as:

$$\mathbf{U}(t) = \sum_{k=-\frac{N}{2}}^{\frac{N}{2}-1} \widehat{\mathbf{U}}_k e^{ik\frac{2\pi}{T}n\Delta t} + \bar{\mathbf{U}}(t) \tag{11}$$

where the slowly varying mean flow is approximated by a collocation method using a polynomial basis set as:

$$\bar{\mathbf{U}}(t) = \phi_{12}(t)\mathbf{U}^{m+1} + \phi_{11}(t)\mathbf{U}^m \tag{12}$$

for a linear variation and

$$\bar{\mathbf{U}}(t) = \phi_{23}(t)\mathbf{U}^{m+1} + \phi_{22}(t)\mathbf{U}^m + \phi_{21}(t)\mathbf{U}^{m-1} \tag{13}$$

for a quadratic variation in time. Here $\mathbf{U}^m$ and $\mathbf{U}^{m+1}$ represent discrete solution instances in time usually taken as the beginning and ending points of the considered period in the quasi-periodic motion (and $\mathbf{U}^{m-1}$ corresponds to the beginning point of the previous period). In the first case, $\phi_{12}(t)$ and $\phi_{11}(t)$ correspond to the linear interpolation functions given by:

$$\phi_{11}(t) = \frac{t^{m+1} - t}{T} \tag{14}$$

$$\phi_{12}(t) = \frac{t - t^m}{T} \tag{15}$$

with the period given as $T = t^{m+1} - t^m$. Similarly, the $\phi_{23}(t), \phi_{22}(t), \phi_{21}(t)$ are given by the corresponding quadratic interpolation functions. Note that in this case, the collocation approximation leads to the determination of the Fourier coefficients as:

$$\widehat{\mathbf{U}}_k = \frac{1}{N}\sum_{n=0}^{N-1} \tilde{\mathbf{U}}^n e^{-ik\frac{2\pi}{T}n\Delta t} \tag{16}$$

with $\tilde{\mathbf{U}}^n = \mathbf{U}^n - \bar{\mathbf{U}}^n$ defined as the remaining periodic component of the function after polynomial subtraction. Differentiating equation (11) and making use of equations (9) and (16) we obtain the following

expression for the time derivative:

$$\frac{\partial}{\partial t}(\mathbf{U}^n) = \sum_{j=0}^{N-1} d_n^j \tilde{\mathbf{U}}^j + \phi'_{12}(t_n)\mathbf{U}^{m+1} + \phi'_{11}(t_n)\mathbf{U}^m \tag{17}$$

for the case of a linear polynomial functions in time. The $\phi'_{12}(t_n)$ and $\phi'_{11}(t_n)$ represent the time derivatives of the polynomial basis functions (resulting in the constant values $\frac{-1}{T}$ and $\frac{1}{T}$ in this case), and the various time instances are given by:

$$t_j = t_m + \frac{j}{N}(t_{m+1} - t_m), \qquad j = 0, \ldots, N-1$$

We also note that $\bar{\mathbf{U}}(t_m) = \mathbf{U}^m = \mathbf{U}(t_m)$ and thus we have $\tilde{\mathbf{U}}^0 = 0$. In other words, the constant mode in the spectral representation must be taken as zero, since it is contained in the polynomial component of the function representation. Therefore, the $j = 0$ component in the summation can be dropped, and rewriting equation (17) in terms of the original time instances $\mathbf{U}^n$ we obtain:

$$\frac{\partial}{\partial t}(\mathbf{U}^n) = \sum_{j=1}^{N-1} d_n^j \mathbf{U}^j - (\sum_{j=1}^{N-1} d_n^j \phi_{12}(t_j) - \phi'_{12}(t_n))\mathbf{U}^{m+1} - (\sum_{j=1}^{N-1} d_n^j \phi_{11}(t_j) - \phi'_{11}(t_n))\mathbf{U}^m \tag{18}$$

Finally, the above expression for the time derivative is substituted into equation (5) which is then required to hold exactly at time instances $j = 1, 2, ..., N-1$ and $j = N$ (which corresponds to the $m+1$ time instance):

$$\sum_{j=1}^{N-1} d_n^j V^j \mathbf{U}^j - (\sum_{j=1}^{N-1} d_n^j \phi_{12}(t_j) - \phi'_{12}(t_n))V^{m+1}\mathbf{U}^{m+1} - (\sum_{j=1}^{N-1} d_n^j \phi_{11}(t_j) - \phi'_{11}(t_n))V^m\mathbf{U}^m \tag{19}$$
$$+\mathbf{R}(\mathbf{U^n}, \dot{\mathbf{x}}^\mathbf{n}, \tilde{\mathbf{n}}^\mathbf{n}) + \mathbf{S}(\mathbf{U^n}, \tilde{\mathbf{n}}^\mathbf{n}) = 0 \qquad n = 1, 2, ..., N$$

As previously, we have N coupled equations with N unknown time instances, although in this case the $j = 0$ time instance which corresponds to the $\mathbf{U}^m$ values are known from the solution of the previous period, while the $j = N$ or $\mathbf{U}^{m+1}$ values are not known, since these are not equal to the $j = 0$ values as they would be in a purely periodic flow. In the case of vanishing periodic content, summation terms involving the d_n^j coefficients vanish by virtue of equation (17) with $\tilde{\mathbf{U}}^j = 0$ and it is easily verified that the above formulation reduces to a first-order backwards difference scheme with a time step equal to the period T. On the other hand, for purely periodic motion, we have $\mathbf{U}^{m+1} = \mathbf{U}^m$ which results in cancellation of the polynomial derivative terms $\phi'_{12}(t_n)$ and $\phi'_{11}(t_n)$. Furthermore, using the identities $\phi_{12}(t_j) + \phi_{11}(t_j) = 1$, and $\sum_{j=0}^{N-1} d_n^j = 0$, it can be seen that the remaining polynomial terms reduce to the missing $j = 0$ instance in the summation. Given the equality $\mathbf{U}^{m+1} = \mathbf{U}^m$, the last equation at $j = N$ becomes identical to the $j = 0$ equation and the time-spectral method given by equation (10) is recovered.

In this description we have used linear polynomials corresponding to a BDF1 time-stepping scheme for clarity. In practice, BDF2 time-stepping schemes are required for accuracy purposes, and the equivalent scheme based on quadratic polynomials is given as:

$$\sum_{j=1}^{N-1} d_n^j V^j \mathbf{U}^j - (\sum_{j=1}^{N-1} d_n^j \phi_{23}(t_j) - \phi'_{23}(t_n))V^{m+1}\mathbf{U}^{m+1} \tag{20}$$
$$-(\sum_{j=1}^{N-1} d_n^j \phi_{22}(t_j) - \phi'_{22}(t_n))V^m\mathbf{U}^m - (\sum_{j=1}^{N-1} d_n^j \phi_{21}(t_j) - \phi'_{21}(t_n))V^{m-1}\mathbf{U}^{m-1}$$
$$+\mathbf{R}(\mathbf{U^n}, \dot{\mathbf{x}}^\mathbf{n}, \tilde{\mathbf{n}}^\mathbf{n}) + \mathbf{S}(\mathbf{U^n}, \tilde{\mathbf{n}}^\mathbf{n}) = 0 \qquad n = 1, 2, ..., N$$

where the values $\mathbf{U}^{m-1}$ and $\mathbf{U}^m$, which correspond to the time instances at the beginning and end of the previous period are known from the solution of earlier periods, and $\mathbf{U}^{m+1} = \mathbf{U}^N$ as previously.

D. Geometric Conservation Law

The geometric conservation law states that in order to maintain discrete conservation, equations (10) and/or (20) must preserve uniform flow as an exact (discrete) solution.[9,19] Substituting $\mathbf{U}^n = \textit{constant}$ into

equation (20) the $\mathbf{R}$ operator reduces to the ALE term (i.e. second term in second integral in equation (4)), and the $\mathbf{S}$ operator vanishes due to its dependence on gradients of $\mathbf{U}$, yielding the following constraint for the face-integrated grid speeds in the case of the BDF/time-spectral method:

$$\sum_{CVFaces} \dot{\mathbf{x}}^{\mathbf{n}} \cdot \tilde{\mathbf{n}}^{\mathbf{n}} = \sum_{j=1}^{N-1} d_n^j V^j - (\sum_{j=1}^{N-1} d_n^j \phi_{23}(t_j) - \phi'_{23}(t_n)) V^{m+1} \tag{21}$$
$$-(\sum_{j=1}^{N-1} d_n^j \phi_{22}(t_j) - \phi'_{22}(t_n)) V^m - (\sum_{j=1}^{N-1} d_n^j \phi_{21}(t_j) - \phi'_{21}(t_n)) V^{m-1}$$

where the sum on the left hand side is over the faces which delimit the cell or control volume V^j. The right hand side of this equation represents a known quantity, since the cell volumes at each time instance are computable given the known grid point locations. However, equation (21) does not in itself enable the prescription of the face integrated grid speeds, since there are more grid faces than volumes. However, the change in volume of a cell from one instance in time to another can be re-written as a sum of the volumes swept by each constituent face:

$$V_j = V_0 + \sum_e F_e^j \qquad\qquad j = 0, 1, 2, 3 \tag{22}$$

where F_e^j is the volume swept by face e from time level 0 to j. Following references,[19,31] we substitute the above form for the volumes into the right hand side of equation (21) and require that the equality hold for each face individually, leading to the GCL formula for computing the face integrated grid speeds $v_g = \dot{\mathbf{x}}^{\mathbf{n}} \cdot \tilde{\mathbf{n}}^{\mathbf{n}}$:

$$v_g = \sum_{j=1}^{N-1} d_n^j F^j - (\sum_{j=1}^{N-1} d_n^j \phi_{23}(t_j) - \phi'_{23}(t_n)) F^{m+1} - (\sum_{j=1}^{N-1} d_n^j \phi_{22}(t_j) - \phi'_{22}(t_n)) F^m - (\sum_{j=1}^{N-1} d_n^j \phi_{21}(t_j) - \phi'_{21}(t_n)) F^{m-1} \tag{23}$$

The face swept volumes F^j and F^m are computed by discretizing the trajectories of the faces between the two time levels into a large number of discrete steps (usually of the order of 60 per period) and computing the volume swept between each step using a two-point integration rule in time, as discussed in references.[9,19]

For purely periodic flows, applying the same approach to the time-spectral scheme (i.e. equation 10) results in the GCL statement:

$$v_g = \dot{\mathbf{x}}^{\mathbf{n}} \cdot \tilde{\mathbf{n}}^{\mathbf{n}} = \sum_{j=0}^{N-1} d_n^j F^j \tag{24}$$

It has been verified that computing the grid speed terms in this manner for a periodic problem indeed satisfies the GCL (i.e. preserves uniform flow discretely). However, the resulting grid speeds are not consistent, in the sense that they do not converge to the exact grid speeds in cases where these are defined analytically. This is illustrated in Figure 1(a), where the analytic grid speed at the tip of the UH-60 rotor in forward flight is compared with the values obtained using N=11 and N=31 time instances using equation (24). The problem arises from the fact that, although we have $V^0 = V^N$, the $F^{j=0}$ swept volumes are identically zero whereas the $F^{j=N}$ volumes are non-zero, violating the periodic nature of the formulation. Recalling that in the BDF/time-spectral formulation the $j = 0$ instance is not used directly, we return to the BDF/time-spectral GCL formulation. Using the simpler BDF1 formulation obtained by inserting a uniform flow into equation (19), we obtain:

$$v_g = \sum_{j=1}^{N-1} d_n^j F^j - (\sum_{j=1}^{N-1} d_n^j \phi_{12}(t_j) - \phi'_{12}(t_n)) F^{m+1} - (\sum_{j=1}^{N-1} d_n^j \phi_{11}(t_j) - \phi'_{11}(t_n)) F^m \tag{25}$$

Using the identities $F^m = 0$ and $F^{m+1} = F^{j=N}$, and the properties of the d_n^J coefficients and linear (in time) ϕ basis functions, we obtain:

$$v_g = d_n^0 F^N + \sum_{j=1}^{N-1} d_n^j F^j \tag{26}$$

where the coefficients $\bar{d}_n^0$ are given by:

$$\bar{d}_n^0 = \frac{1}{T} - \sum_{j=1}^{N-1} \frac{j d_n^j}{N} \tag{27}$$

Applying this formula for computing the grid speeds for the periodic UH-60 forward flight geometry results in accurate and converging grid speeds compared with analytic values, as shown in Figure 1(b).

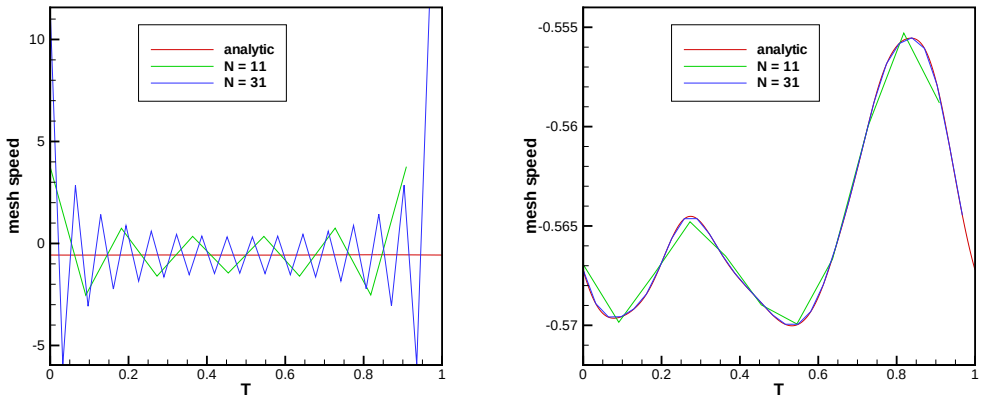

(a) Inconsistent (equation (24))

(b) Consistent (equation (26))

Figure 1. Comparison of analytic and GCL compliant grid speeds for the periodic UH60 forward flight flexible rotor case. Note different scales for both plots.

E. Fully Implicit Method

Similar to the dual time-stepping method used to solve implicit time-domain problems (for example using backwards difference time discretizations), a pseudo-time τ can be added to equations (10) and (20) in order to formulate an iterative solution procedure, for example, equation (10) becomes:

$$\frac{\partial}{\partial \tau}(V^n \mathbf{U}^n) + \sum_{j=0}^{N-1} d_n^j V^j \mathbf{U}^j + \mathbf{R}(\mathbf{U^n}, \dot{\mathbf{x}}^\mathbf{n}, \tilde{\mathbf{n}}^\mathbf{n}) + \mathbf{S}(\mathbf{U^n}, \tilde{\mathbf{n}}^\mathbf{n}) = 0 \tag{28}$$

According to reference,[30] the maximum stable pseudo-time step can be computed as

$$\Delta\tau = CFL \frac{V}{\parallel \lambda \parallel + \frac{N}{2} V} \tag{29}$$

where λ is the spectral radius of the flux Jacobian. By using the implicit backward Euler method in pseudo time, equation (28) can be written as:

$$\mathbf{A}\Delta\mathbf{U} = -\sum_{j=0}^{N-1} d_n^j V^j \mathbf{U}^j - \mathbf{R}(\mathbf{U^n}, \dot{\mathbf{x}}^\mathbf{n}, \tilde{\mathbf{n}}^\mathbf{n}) - \mathbf{S}(\mathbf{U^n}, \tilde{\mathbf{n}}^\mathbf{n}) \tag{30}$$

where, for the fully coupled implicit method, the matrix $\mathbf{A}$ takes the form:[25]

$$\mathbf{A} = \begin{bmatrix} \frac{V^0}{\Delta\tau_0}\mathbf{I} + \mathbf{J_0} & V^1 d_0^1 \mathbf{I} & \dots & V^{N-1} d_0^{N-1} \mathbf{I} \\ V^0 d_1^0 \mathbf{I} & \frac{V^1}{\Delta\tau_1}\mathbf{I} + \mathbf{J_1} & \dots & V^{N-1} d_1^{N-1} \mathbf{I} \\ \vdots & \vdots & \dots & \vdots \\ V^0 d_{N-1}^0 \mathbf{I} & V^1 d_{N-1}^1 \mathbf{I} & \dots & \frac{V^{N-1}}{\Delta\tau_{N-1}}\mathbf{I} + \mathbf{J_{N-1}} \end{bmatrix} \tag{31}$$

where **J** corresponds to the flux Jacobians. Keeping only the diagonal terms in this matrix and discarding all other terms corresponds to a local implicit method. On the other hand, if all terms are retained, and a block Jacobi strategy is used to solve equation (30), a fully implicit solution strategy which takes into account the coupling between all time instances is obtained. Note that these off-diagonal blocks in the **A** matrix are rather simple, as they involve a scalar multiplication of the identity matrix. However, the size of each block corresponds to a complete spatial field for one time instance. The fully implicit method can be implemented with little additional memory and requires only a small amount of additional floating point operations. However, for parallel implementations, each time instance solution must broadcast its entire solution field to all other solution instances. In order to reduce overall communication, this coupling is performed at the end of every multigrid cycle, rather than after each iterative smoothing cycle.

III. Results and Discussion

A. UH-60A Maneuver Description

The objective of this work is to investigate the effectiveness of the BDF/time-spectral approach originally proposed in reference[20] for important practical rotorcraft problems that are not fully periodic. Simulation of the Utility Tactical Transport Aerial System (UTTAS) pull-up maneuver of the UH-60A helicopter constitutes an ideal test case for this purpose. Detailed measurements of blade aerodynamics and structural dynamics load measurements have been conducted on this configuration as part of the NASA-Army UH-60A Airloads Program which investigated a wide range of flight conditions. An extensive documentation of the flight test program can be found in Bousman and Kufeld .[5,14] The operating envelope of the helicopter plotted as variation of vehicle weight coefficient with advance ratio is shown in Figure 2. The limiting factors for these flight conditions are the maximum thrust limit because of retreating blade stall and maximum sectional airfoil lift that can be generated. McHugh et al.[21] determined the maximum thrust boundary using wind-tunnel tests which is represented in the figure. Note that all the steady flight conditions lie below the McHugh boundary. Figure 2 also shows the variation of weight coefficient with advance ratio for the UTTAS pull-up maneuver. The maneuver begins quite close to the maximum level flight speed of the aircraft and achieves a peak load factor of 2.1g, which exceeds the steady state McHugh boundary. Therefore the UTTAS pull-up maneuver is a challenging flight condition in terms of predictive capability.

In this work, we first investigate the periodic condition of high-speed forward flight corresponding to the initial condition for the pull-up maneuver using the pure time-spectral approach, and then proceed to the simulation of the transient pull-up maneuver using the BDF/time-spectral method. This latter case consists of a transition from the initial periodic high speed forward flight condition to a steady climb condition in about 40 revolutions of the rotor (approximately 10 seconds).

In both cases, the UH-60A aircraft is modeled as an isolated flexible rotor. In order to further simplify the problem, we make use of prescribed flight path and prescribed aeroelastic rotor deflections obtained from a fully coupled CFD-CSD simulation performed previously in reference.[28] Figure 3(a) shows the prescribed speed and pitch angle of the hub. Figure 3(b) shows the prescribed displacement and the Wiener-Milenkovic parameters(c1, c2 and c3) used to define the aeroelastic motion of the blade tip.

The prescribed motion is applied in four different operations to the computational mesh. Firstly, the rotational motion if applied by directly rotating the mesh by the required angle about the hub axis. Next, the mesh is pitched as a solid body and translated according to the prescribed hub motion and attitude. Finally, the aeroelastic deflections are applied to the surface grid for each blade, and the interior mesh is then deformed in response to the surface deflections using a spring analogy mesh deformation approach. These operations are performed at each time step in the time-domain (BDF2) simulation, and for each time instance in the time spectral or BDF/time-spectral approach.

Figure 4 illustrates the mesh used for the UH60A rotor in all simulations. The mesh consists of approximately 1.5 million grid points in a single block unstructured mesh about the entire 4-bladed rotor configuration. A hybrid mesh is used, consisting of prismatic elements in the boundary layer regions near the rotor surface and tetrahedral elements elsewhere. All cases consist of a Reynolds-averaged Navier-Stokes simulation using the Spalart-Allmaras turbulence model,[29] with a wall normal spacing of the order of $Y^+ = 1$. Although the mesh is relatively coarse for these simulations, the principal focus of at this preliminary stage is to investigate the agreement between the time-spectral approaches and the time-domain (BDF2) method. For these purposes, the BDF2 simulations were performed using a time step of 1 degree rotation and repeated using a time step of 0.5 degrees. Since minimal differences were observed between these two simulations,

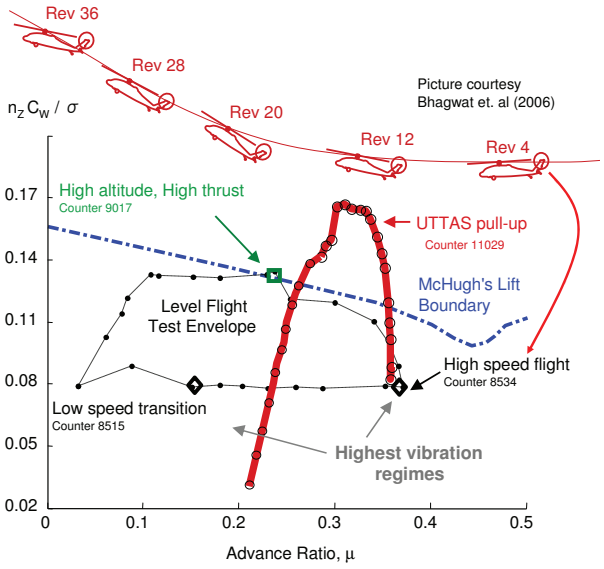

Figure 2. UH-60A flight envelope and maneuver trajectory

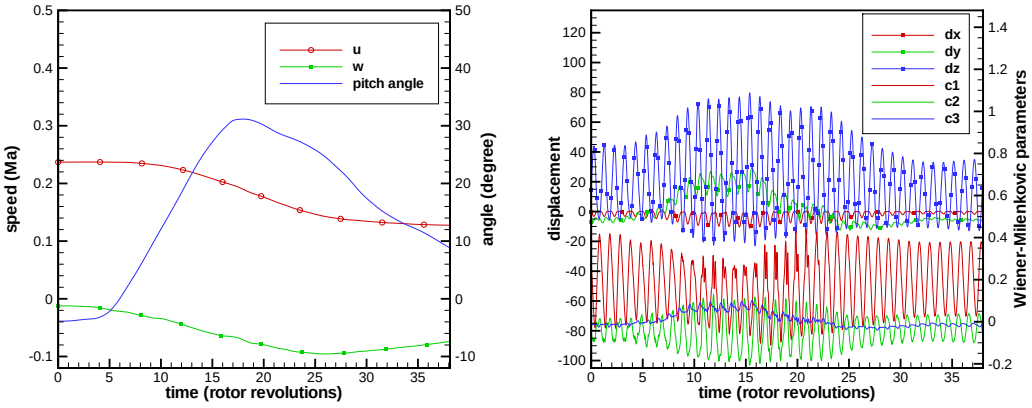

(a) Prescribed hub motion

(b) Displacement and rotation of blade tip

Figure 3. Prescribed motion used for maneuver simulation.

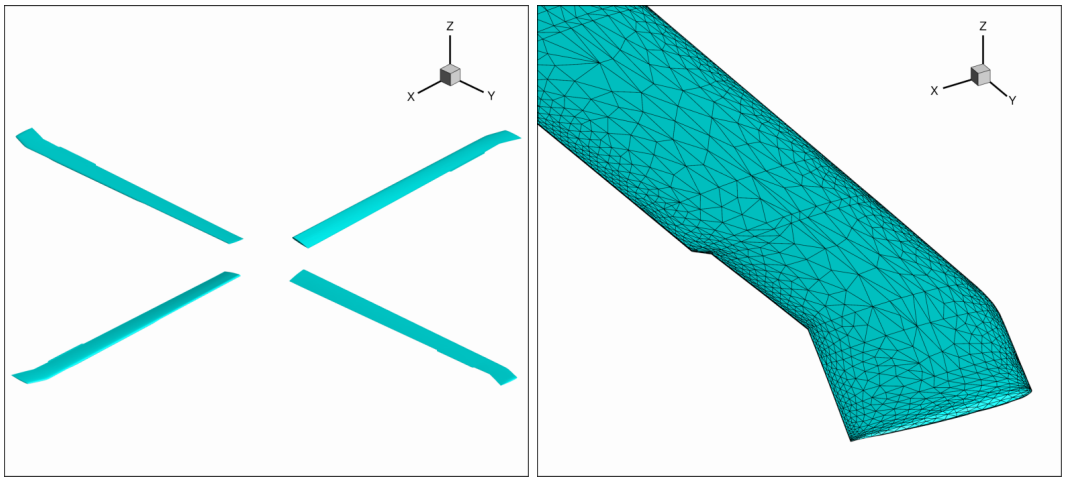

(a) Four blades (b) Mesh near blade tip

Figure 4. Unstructured mesh used for UH60A rotor configuration.

the BDF2 simulations were assumed to be relatively well converged in terms of temporal error, for this mesh size. Similarly, time-spectral and BDF-time-spectral simulations using N=7,9, and 11 time instances were performed and compared with the BDF2 simulations. Where available, comparisons with experimental flight-test data are also given. Although a temporal convergence study has been performed, a spatial mesh convergence study has not been undertaken, and is planned for future work.

B. High Speed Forward Flight Periodic Test Case

Figures 5 and 6 illustrate the results obtained for the high speed forward flight case. Time histories of non-dimensional sectional normal forces (denoted by C_nM^2) and sectional pitching moments (denoted by C_mM^2) from analysis and flight test data are compared in the figures. This flight condition marks the highest speed (158 kts) that can be achieved by the UH-60 blackhawk (denoted by flight 8534 in Figure 2). The non-dimensional parameters for this operating condition are advance ratio μ=0.368, tip Mach number M_{tip}=0.6415 and thrust coefficient C_T=0.00666. The elastic blade motions for this case is obtained from our previous CFD/CSD coupling work.[27]

For this case, the flow and blade motions are fully periodic and the time-spectral approach is used to compute the periodic solution directly. For the time-domain solution, the BDF2 temporal discretization was used with a time step corresponding to 0.5 degrees rotation. In order to obtain the periodic solution, the simulation of three revolutions was performed to flush out the transient behavior. The best agreement between the two schemes was obtained using N=11 time instances in the time-spectral method and is shown in the figures. The general trends in both the blade normal force coefficients and sectional pitching moments are in good agreement between the two methods, although the amplitude of the forces and moments are slightly lower using the time-spectral method. Both simulations agree qualitatively with the experimental flight test data in terms of the location and shape of the major variations in the forces and moments. Discrepancies in terms of the magnitudes of force/moment variations and in terms of some of the finer details of the time histories are noted, and these are attributed at least in part to the spatial grid resolution used in the current study.

C. Transient Pull-Up Maneuver Test Case

The transient test case was simulated using the BDF/time-spectral approach with N=7,9, and 11 time instances. A baseline BDF2 time-domain simulation with a 0.5 degree time step was also performed for comparison purposes. Figures 7(a), 7(b) and 7(c) show the comparison of the predicted forces in x, y and z directions on one blade between BDF and BDFTS with different time instance N. The forces are plotted as functions of time in units of revolution. The forces predicted by BDFTS show generally good agreement with the results obtained using BDF. Figure 7(d) shows the comparison of the predicted rotor thrust between

BDF, BDFTS and the flight test measurements. The measured data is averaged over each revolution and therefore appears smoother. The pattern and averaged amplitude of the lift predicted by BDF and BDFTS are in agreement with the measured data, although the BDFTS results show larger amplitude oscillations. Comparison of the rotor lift distribution during revolution No. 1 are shown in Figure 8. The lift differences between the measured data and the predicted results by BDFTS are pronounced near the 0 degree azimuth region. One of the reasons for these differences is the relatively coarse mesh used in the simulation. Another possible reason may be the interaction between the blade and the hub/fuselage. Similar deficiencies were observed in the coupled CFD/CSD solutions described in reference.[28] The use of prescribed aeroelastic deflections obtained from this work[28] is also a limiting factor that must be taken into consideration. Future studies should include effects of the aircraft fuselage, hub, engines and the tail rotor.

Figure 9 and Figure 10 show the comparison of the normal force and the pitching moment respectively, at revolution No. 6 of the transient maneuver. The operating condition at this location is still relatively close to the high speed forward flight condition although significant transient effects are evident. The overall sectional normal force and pitching moment are reasonably predicted in this case by both BDF and BDFTS, especially at the inboard radial stations. On the outboard stations there is significant degradation in the agreement with test data and analysis in the advancing blade phase. However, the BDFTS solution is consistent with the BDF solution and approaches the BDF solution with increasing number of modes. Therefore, an improved BDF solution with significant improvements in mesh quality, will most likely result in a similarly improved BDFTS solution.

In Figure 11 and Figure 12 we compare the evolution of dominant harmonics of sectional normal force (mean normal force) and sectional pitching moment (1/rev frequency) with rotor revolution. As the aircraft pitches up during the initial part of the maneuver, the total thrust increases rapidly, reflected in the almost linear increase of sectional lift in all radial stations. All the analyses (BDF and BDFTS with varying mode counts) capture this phenomena qualitatively, even though the beginning magnitudes are not consistent with flight test data. Increasing rotor lift is a key phenomena in the transient maneuver and this behavior is captured equally well by the BDF and BDFTS schemes. The evolution of the 1/rev frequency pitching moments (depicted in Figure 12) show lesser phenomenological agreement with experimental data compared to the normal forces. Certain radial stations (such as r/R=0.965, r/R=0.775, r/R=0.400) show consistent behavior with the flight test data, while other do not. It is worth noting that the relative variations in 1/rev sectional pitching moment are much smaller compared to that observed in the mean sectional normal forces. The coarse mesh system used throughout this paper has been observed to be inaccurate in prediction of detailed aerodynamic loading even with the traditional BDF approach. Hence, it is expected that the discrepancies will be much more pronounced in the pitching moment prediction, as the pitching moments are more sensitive to variation of the surface pressure distribution.

D. Computational Efficiency

Precise comparison of computational efficiency between the time-domain and time-spectral methods would require a complete quantification of the temporal accuracies of both approaches in order to be able to compare the cost of these methods for an equivalent level of delivered accuracy. In addition, the level of prescribed convergence tolerance at each implicit time step in the time-domain approach or for each periodic solution in the time-spectral approach governs the cost of each method. In the absence of an exact temporal accuracy and convergence error quantification, we present the computational cost of the methods as used in the present study.

The BDF simulation was conducted on 160 Xeon cores using 20 sub-iterations per time step and 720 time steps per revolution or period. The solution of each implicit time step required approximately 3.6 seconds.

The BDFTS simulations were conducted on 24 x N Xeon cores, where N = 7,9, or 11 corresponds to the number of time instances per period. A total of 200 multigrid sub-iterations were used for the coupled solution of all N time instances at each period or rotor revolution. The time required for the solution of a single period or revolution was 1100, 1300 and 1500 seconds for N = 7, 9 and 11, respectively (on 168, 216 and 264 cores). Assuming perfect speedup, the BDF2 simulation run on the equivalent number of cores requires approximately twice as much total cpu time as the BDFTS method using N=7, although the methods are roughly equivalent in total cpu time for N=11. One of the advantages of the BDFTS approach is the ability to use additional parallelism in the time domain. Thus, if the spatial parallelism is restricted to 160 partitions or cores, the BDFTS simulations can be run on 800, 1120 and 1760 cores (for N=7,9,11 respectively) achieving a wall clock speed up of approximately 10 over a time-domain BDF2 calculation

limited to 160 cores.

IV. Concluding Remarks and Future work

In previous work the BDF/time-spectral approach was introduced as a strategy for extending the applicability of time-spectral methods to problems that are not fully periodic. In the current paper, we have presented the first application of this method to a rotorcraft maneuvering problem of practical interest. The results indicate a consistent behavior between the traditional BDF2 time-domain results and BDF-time-spectral results, with better agreement as the number of time instances is increased in the BDF-time-spectral method. Although reasonable qualitative agreement was obtained between the simulation results and the experimental results obtained from flight test data, significant discrepancies remain. These are attributed in large part to the spatial resolution used for the simulations, and future work will focus on simulations with finer meshes including a grid resolution study. At the same time, the use of more time instances in the time-spectral approach will be examined, and the development of faster implicit system convergence will be pursued. Time-spectral approaches offer the potential for much higher temporal resolution at reduced cost, and enable parallelism to be extracted from the temporal dimension, promising much more efficient overall solution strategies for periodic or quasi-periodic problems. The long term objective of this work is to demonstrate these advantages on rotorcraft problems or practical interest.

V. Acknowledgments

This work was supported under ONR Grant N00014-09-1-1060. We also are thankful to Michael Long for providing the unstructured meshes used in this work.

References

[1]A. Abhishek, A. Datta, and I. Chopra. Comprehensive analysis prediction, and validation of UH60A blade loads in unsteady maneuvering flight. AHS Specialists Conference on Aeromechanics, AHS International, Alexandria, VA, Jan 2008.

[2]M. Bhagwat and R. Ormiston. Examination of rotor aerodynamics in steady and maneuvering flight using CFD and conventional methods. AHS Specialists Conference on Aeromechanics, AHS International, Alexandria, VA, Jan 2008.

[3]M. Bhagwat, R. Ormiston, H. Saberi, and H. Xin. Application of CFD/CSD coupling for analysis of rotorcraft airloads and blade loads in maneuvering flight. 63rd Forum of the American Helicopter Society, AHS International, Alexandria, VA, May 2007.

[4]G. Bousman, R. M. Kufeld, D. Balough, and J. L. Cross. Flight testing the UH-60A in maneuvering flight. Technical report, 50th Annual Forum of the American Helicopter Society, Washington, D.C, May 1994.

[5]G. Bousman, R. M. Kufeld, D. Balough, J. L. Cross, K. F. Studebaker, and C. D. C. D. Jennison. Flight testing the UH-60A airloads aircraft. May 1994. 50th Annual Forum of the American Helicopter Society, Washington, D. C.

[6]C. Canuto, M. Y. Hussaini, A. Quarteroni, and T. A. Zang. *Spectral Methods in Fluid Dynamics*. Springer, 1987.

[7]S. Choi and A. Datta. CFD prediction of rotor loads using time-spectral method and exact fluid-structure interface. AIAA 2008-7325, Aug. 2008.

[8]S. Choi, M. Potsdam, K. Lee, G. Iaccarino, and J. J. Alonso. Helicopter rotor design using a time-spectral and adjoint-based method. AIAA 2008-5810, Sep. 2008.

[9]P. Geuzaine, C. Grandmont, and C. Farhat. Design and analysis of ALE schemes with provable second-order time-accuracy for inviscid and viscous flow simulations. *Journal of Computational Physics*, 191(1):206–227, 2003.

[10]A. K. Gopinath and A. Jameson. Time spectral method for periodic unsteady computations over two- and three-dimensional bodies. AIAA Paper 2005-1220, Jan. 2005.

[11]D. Gottlieb and S. A. Orszag. Numerical analysis of spectral methods: Theory and applications. CBMS-26, Regional Conference Series in Applied Mathematics, SIAM,Philadelphia, PA, 1977.

[12]K. C. Hall, J. P. Thomas, and W. S. Clark. Computation of unsteady nonlinear flows in cascades using a harmonic balance technique. *AIAA Journal*, 40(5):879–886, 2002.

[13]J. Hesthaven, S. Gottlieb, and D. Gottlieb. *Spectral Methods for Time-Dependent Problems*. Cambridge Monographs on Applied and Computational Mathematics, 2007.

[14]R. M. Kufeld. High load conditions measured on a UH-60A in maneuvering flight. *Journal of the American Helicopter Society*, 43(3):202–211, July 1998.

[15]C. Lanczos. Discourse on Fourier series. Hafner, New York, 1966.

[16]K.-H. Lee, J. J. Alonso, and E. van der Weide. Mesh adaptation criteria for unsteady periodic flows using a discrete adjoint time-spectral formulation. AIAA paper 2006-0692, Jan. 2006.

[17]D. J. Mavriplis and S. Pirzadeh. Large-scale parallel unstructured mesh computations for 3D high-lift analysis. *AIAA Journal of Aircraft*, 36(6):987–998, Dec. 1999.

[18]D. J. Mavriplis and V. Venkatakrishnan. A unified multigrid solver for the Navier-Stokes equations on mixed element meshes. *International Journal for Computational Fluid Dynamics*, 8:247–263, 1997.

[19]D. J. Mavriplis and Z. Yang. Construction of the discrete geometric conservation law for high-order time accurate simulations on dynamic meshes. *Journal of Computational Physics*, 213(2):557–573, 2006.

[20]D. J. Mavriplis and Z. Yang. Time spectral method for quasi-periodic unsteady computation on unstructured meshes. AIAA Paper 2010-5034, June 2010.

[21]F. J. McHugh. What are the lift and propulsive force limits at high speeed for the conventional rotor ? May 1978. American Helicopter Society 34th Annual Forum, Washinton D.C.

[22]M. McMullen, A. Jameson, and J. J. Alonso. Acceleration of convergence to a periodic steady state in turbomachineary flows. AIAA Paper 2001-0152, Jan. 2001.

[23]M. McMullen, A. Jameson, and J. J. Alonso. Application of a non-linear frequency domain solver to the Euler and Navier-Stokes equations. AIAA Paper 2002-0120, Jan. 2002.

[24]S. Sankaran, A. Gopinath, E. V. D. Weide, C. Tomlin, and A. Jameson. Aerodynamics and flight control of flapping wing flight vehicles: A preliminary computational study. AIAA 2005-0841, Jan. 2005.

[25]F. Sicot, G. Puigt, and M. Montagnac. Block-jacobi implicit algorithm for the time spectral method. *AIAA Journal*, 46(12):3080–3089, 2008.

[26]B. Silbaugh and J. D. Baeder. Coupled CFD/CSD analysis of a maneuvering rotor using staggered and time-accurate coupling schemes. AHS Specialists Conference on Aeromechanics, AHS International, Alexandria, VA, Jan 2008.

[27]J. Sitaraman and J. D. Baeder. Evaluation of the wake prediction methodologies used in CFD based rotor airload computations. 24th AIAA Conference on Applied Aerodynamics, San Francisco, CA., June 2006.

[28]J. Sitaraman and B. Roget. Prediction of helicopter maneuver loads using a fluid-structure analysis. *Journal of Aircraft*, 46(5):1770–1784, 2009.

[29]P. R. Spalart and S. R. Allmaras. A one-equation turbulence model for aerodynamic flows. AIAA 1992-0439, Jan. 1992.

[30]E. van der Weide, A. K. Gopinath, and A. Jameson. Turbomachineary applications with the time spectral method. AIAA Paper 2005-4905, June 2005.

[31]A. van Zuijlen and H. Bijl. High order time integration for fluid-structure interaction on moving meshes. AIAA paper 2005-5247, June 2005.

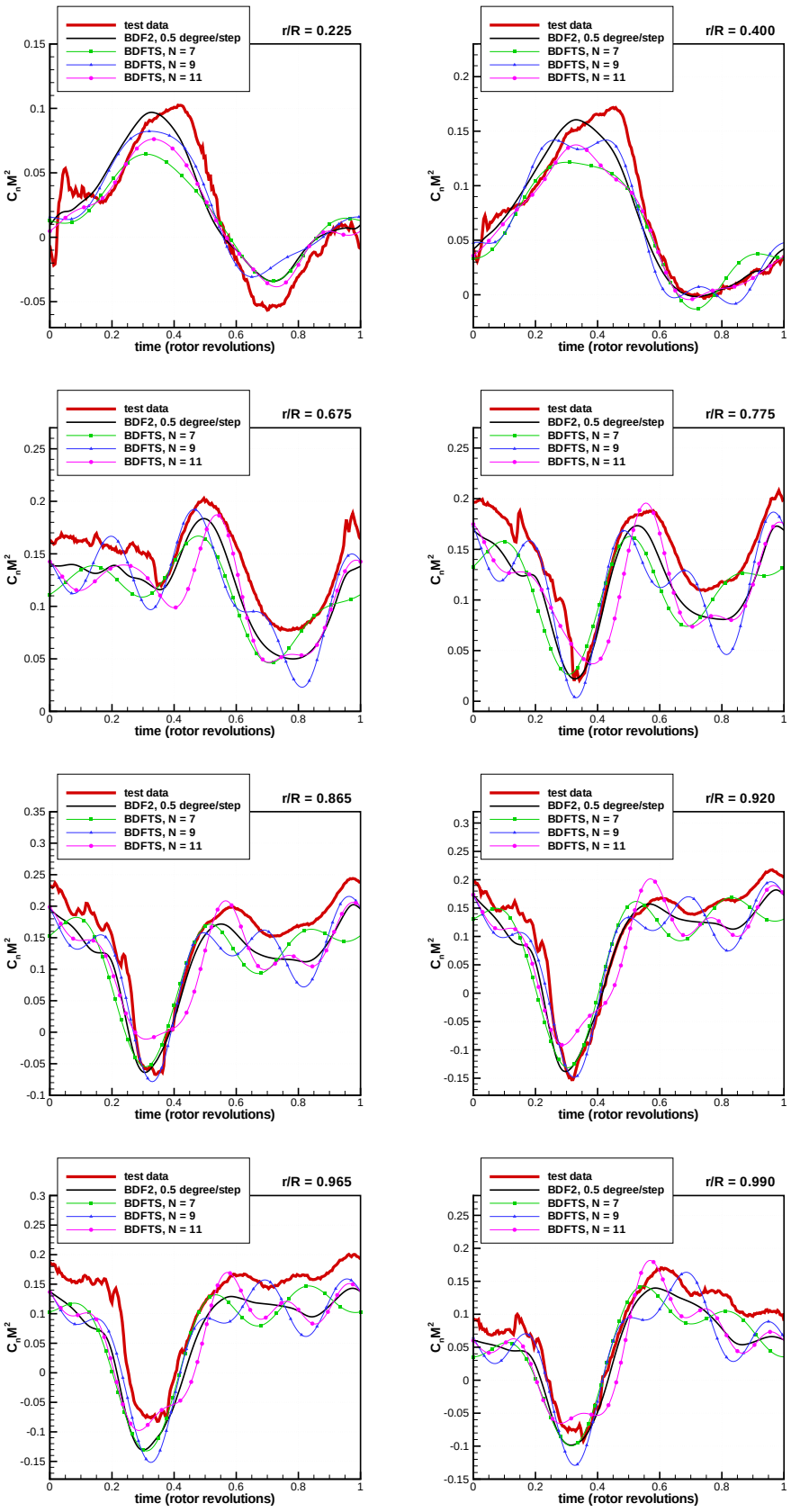

Figure 5. Comparison of blade normal force coefficients for high speed forward flight periodic case using time-spectral approach with 11 time instances versus BDF2 methods using a time step of 0.5 degrees

.

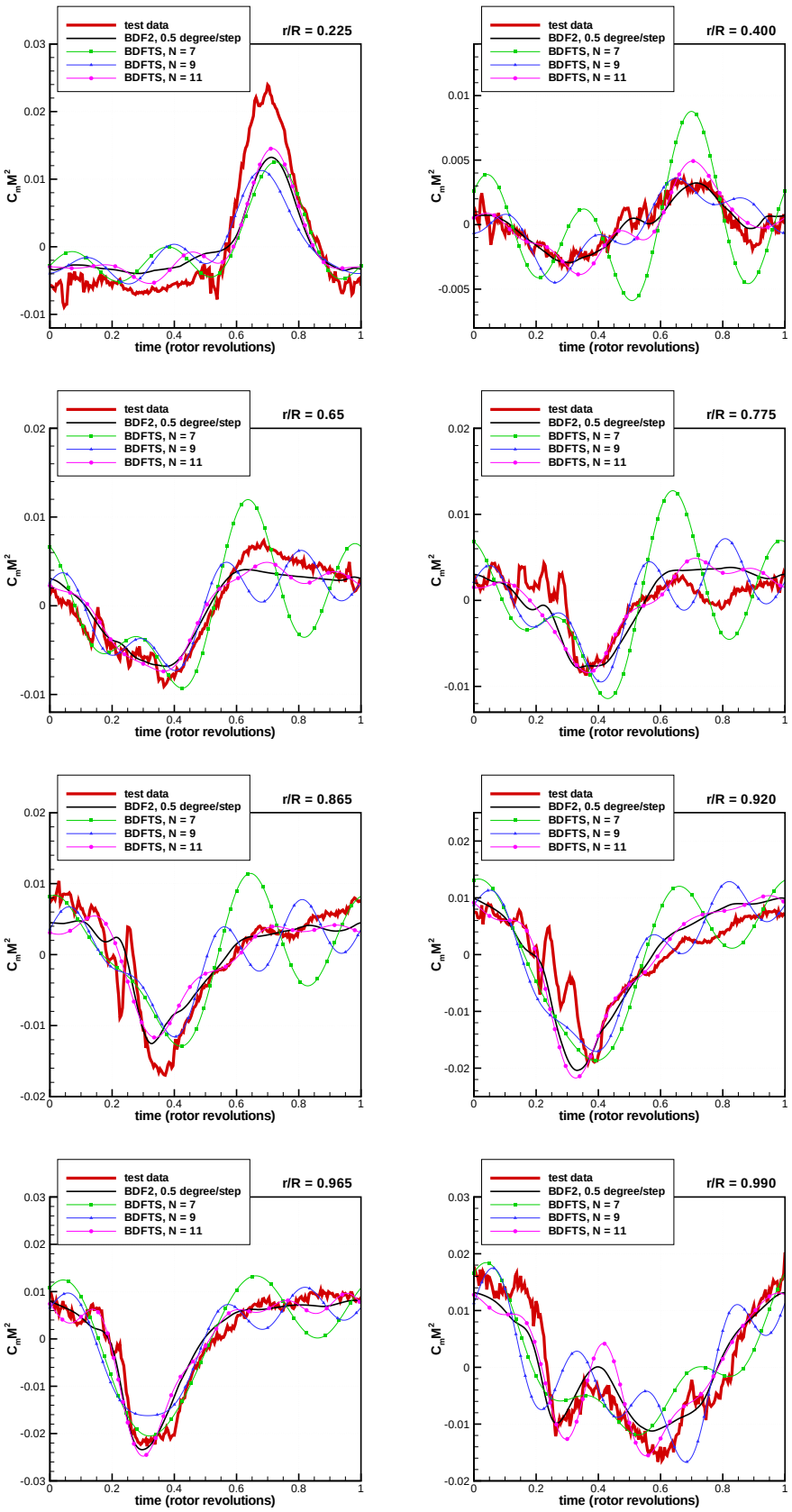

Figure 6. Comparison of blade pitching moments for high speed forward flight periodic case using time-spectral approach with 11 time instances versus BDF2 methods using a time step of 0.5 degrees

.

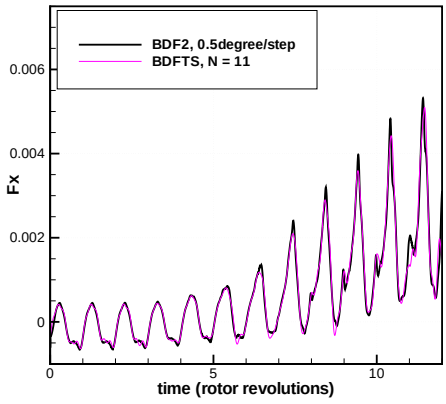

(a) force in x direction on one blade

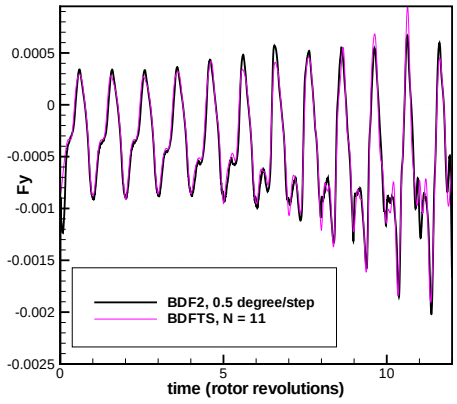

(b) force in y direction on one blade

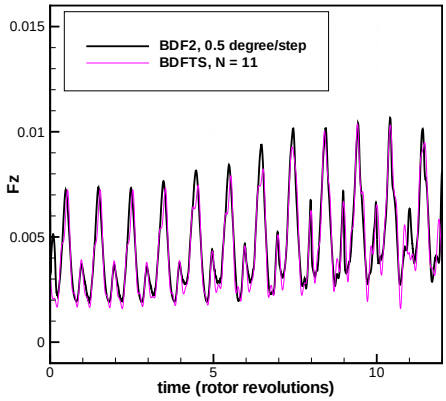

(c) force in z direction on one blade

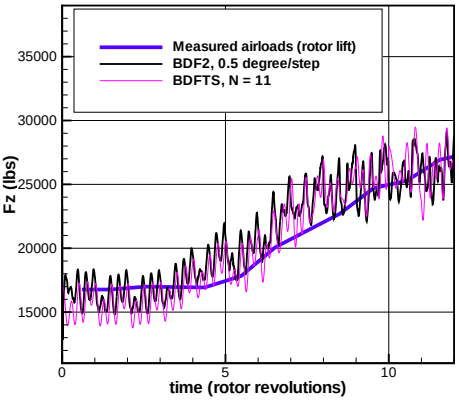

(d) total lift

Figure 7. Force comparison between time-domain BDF2 method and BDF-time-spectral method for transient UH60A pull-up maneuver including flight test data.

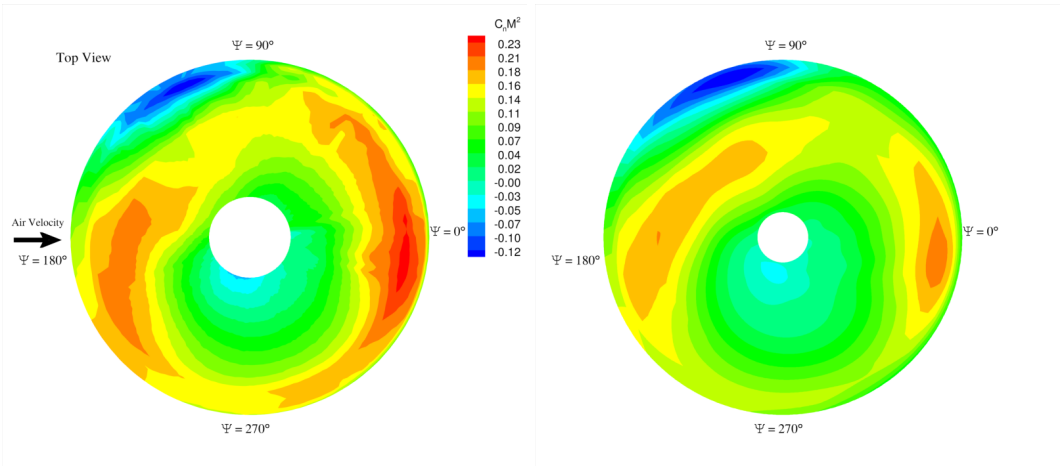

(a) test data

(b) BDF

(c) BDFTS, N=7

(d) BDFTS, N=9

(e) BDFTS, N=11

Figure 8. Contours of rotor lift (sectional normal force) for revolution No.1.

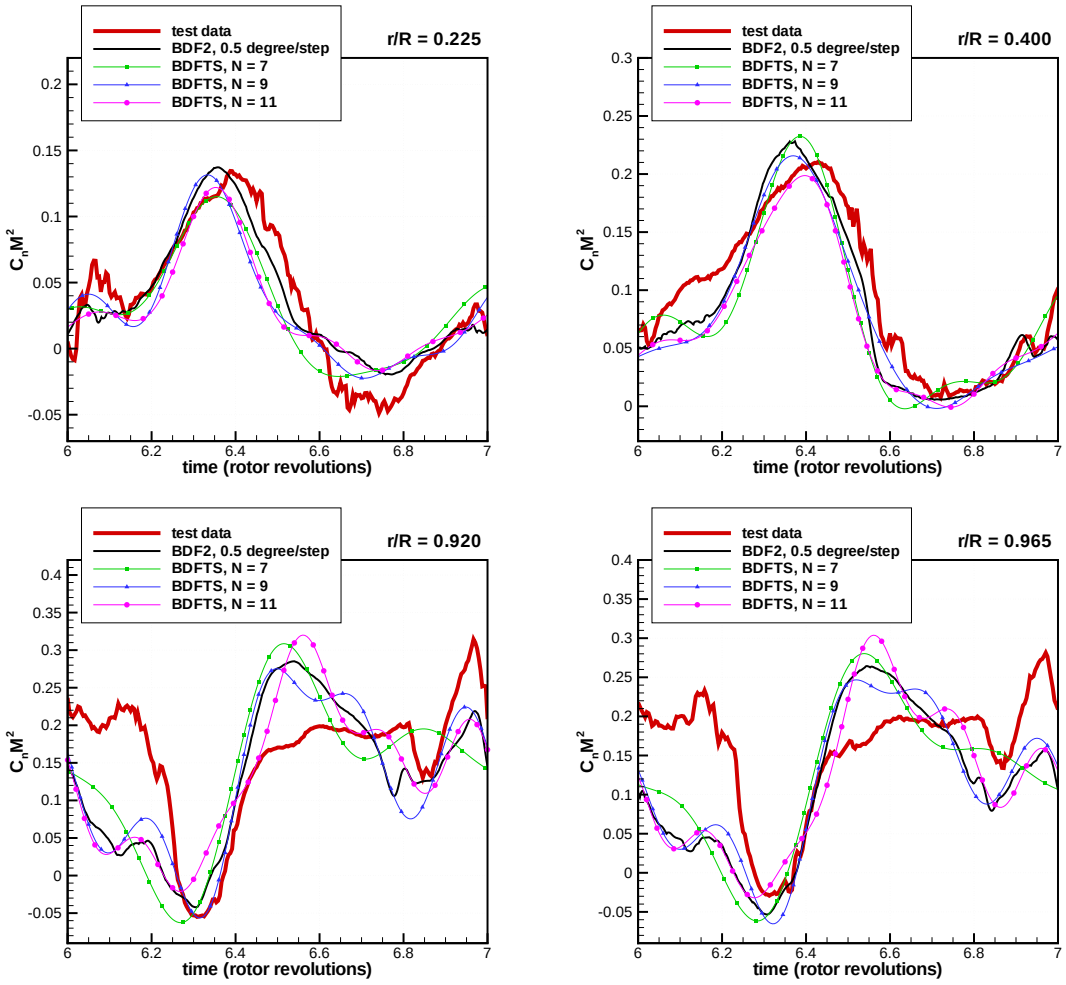

Figure 9. Nondimensional section normal force vs the azimuth angle at revolution 6.

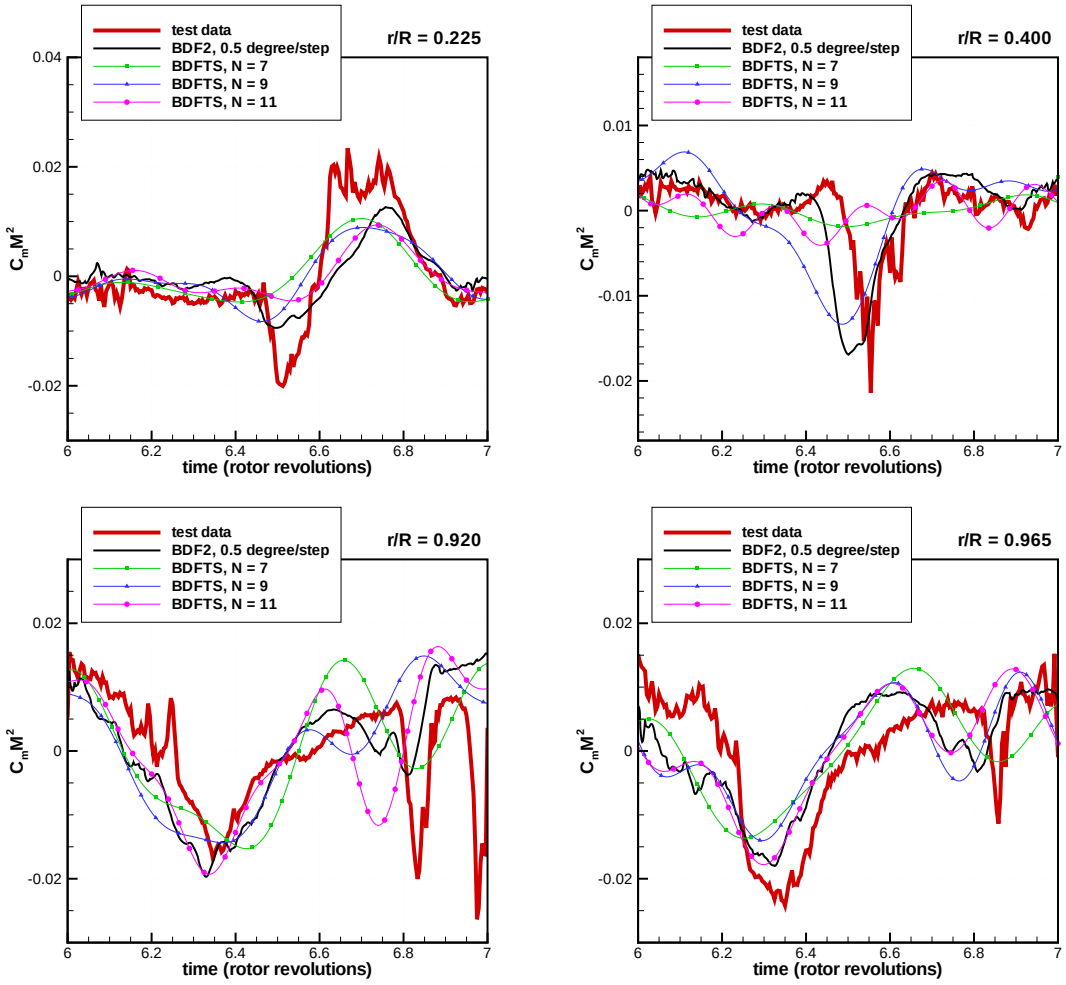

Figure 10. Nondimensional section pitching moment(mean removed) vs the azimuth angle at revolution 6.

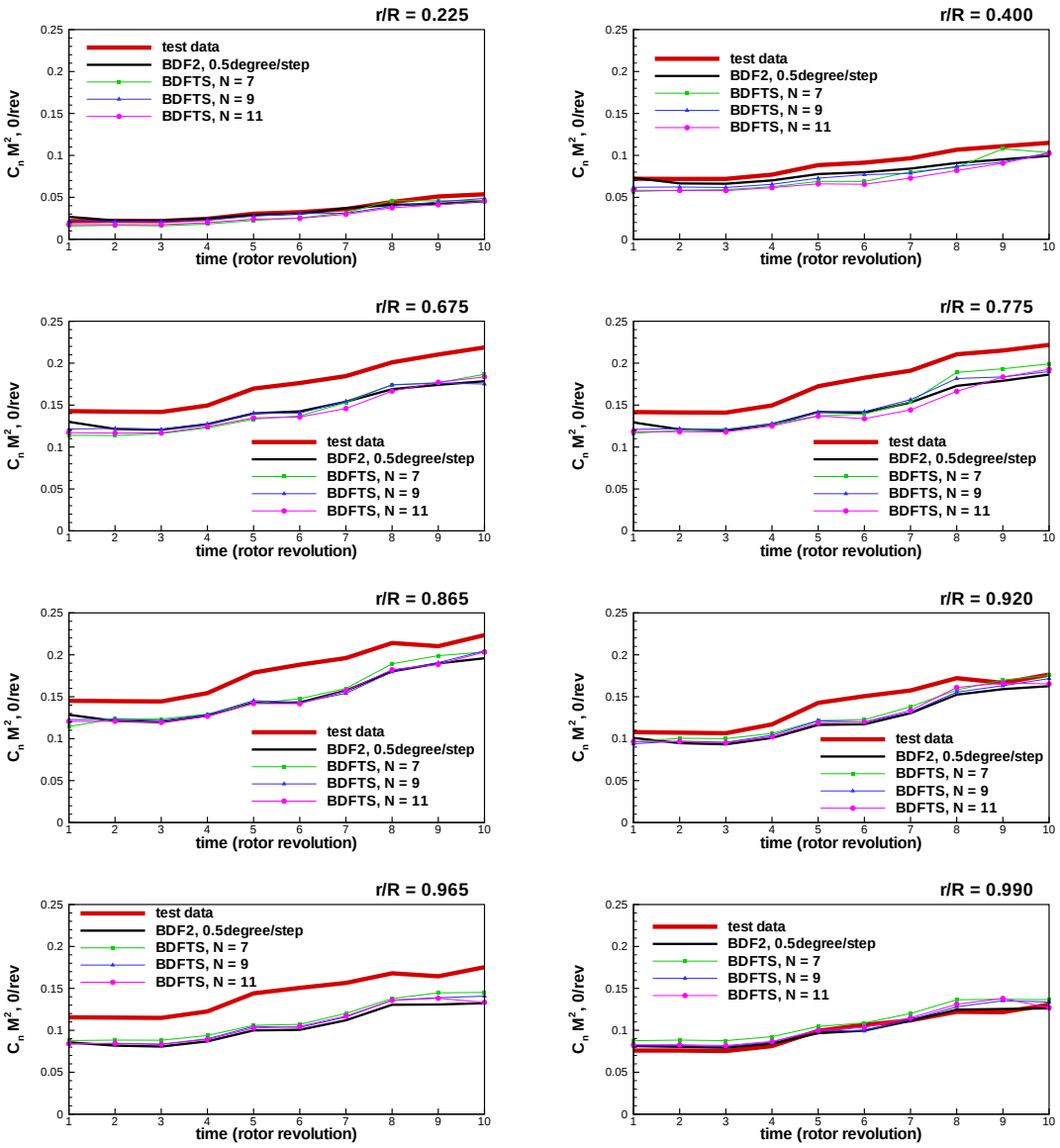

Figure 11. Nondimensional section normal force comparison in frequency domain for UH60A pull up maneuver over first 10 revolutions.

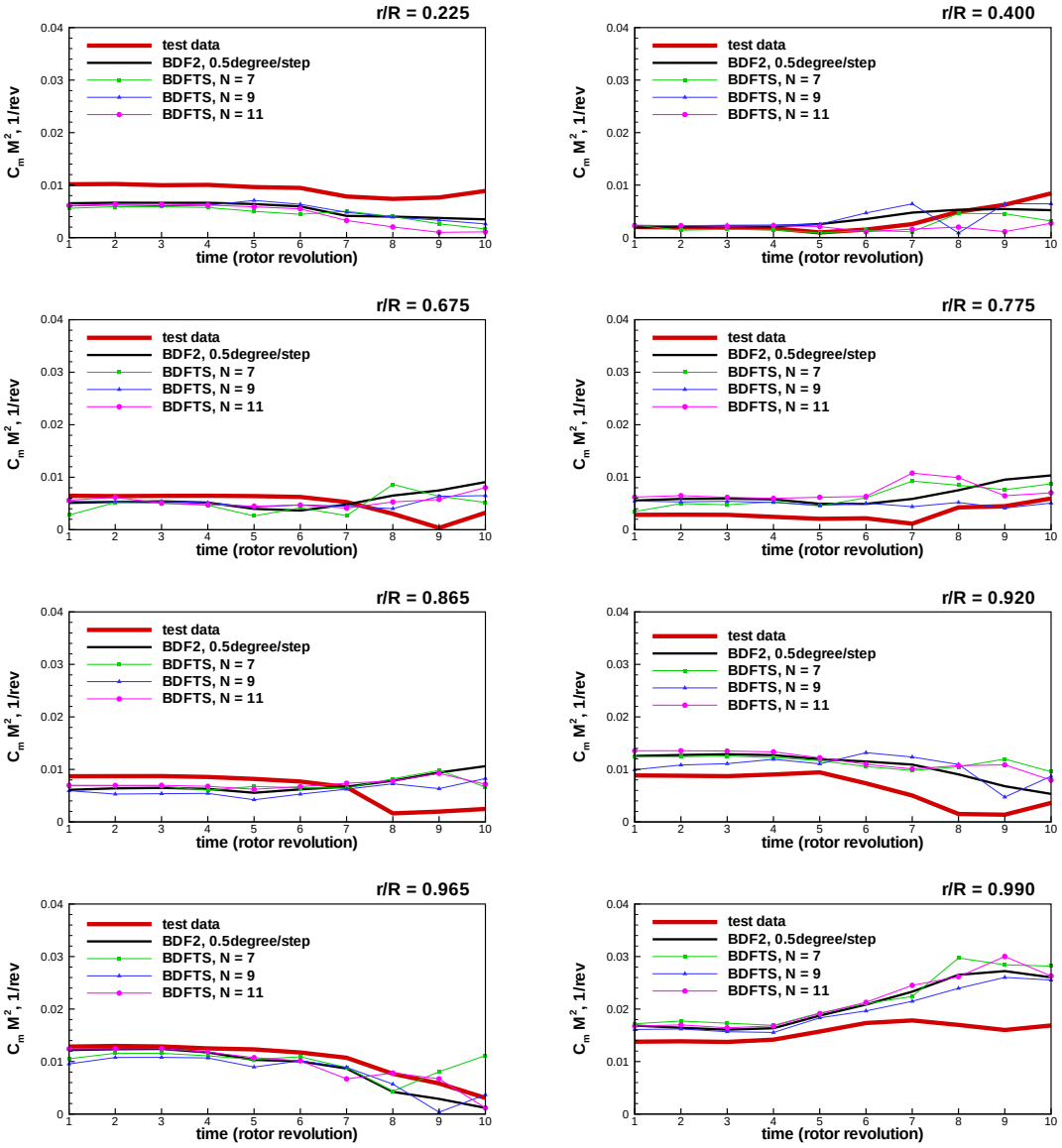

Figure 12. Nondimensional section pitching moment(mean removed) comparison in frequency domain for UH60A pull up maneuver over first 10 revolutions.